

Numerical solution of the Fokker-Planck equation with electric field and collisions

Matt Landreman*

Plasma Science and Fusion Center, MIT, Cambridge, MA, 02139, USA

Adam Stahl and Tünde Fülöp

*Department of Applied Physics, Nuclear Engineering,
Chalmers University of Technology and Euratom-VR Association, Göteborg, Sweden*

(Dated: June 6, 2019)

An efficient numerical method is demonstrated for solving the Fokker-Planck equation for the electron distribution function in the presence of an electric field of arbitrary strength. The approach is continuum (Eulerian), and we employ a relativistic collision operator, valid for arbitrary energies. Both primary and secondary runaway electron generation are included. For primary generation, a time-independent formulation of the problem is described, requiring only the solution of a single sparse linear system. As an application, the electron distribution function is used for calculating the synchrotron emission spectrum of the runaways.

I. INTRODUCTION

Interactions between Coulomb collisions and electric fields are important in many areas of plasma physics, ranging from laser-plasma particle acceleration and tokamak disruptions to solar flares and lightning discharges. One of the most interesting of these collisional effects in plasmas is the runaway acceleration of particles: due to the decrease in the Coulomb collision cross section with velocity, charged particles can be accelerated by an electric field to high energies. In tokamaks, the resulting energetic particles can damage plasma-facing components and are expected to be a significant danger in the upcoming ITER experiment. Electrons are typically the species for which runaway is most significant[1, 2], but runaway

*landrema@mit.edu

ions [3] and positrons [4, 5] can also be produced. Relatively large electric fields are required for runaway production, and in tokamaks these can arise during disruptions or in sawtooth events. Understanding of runaway electrons and their generation and mitigation is essential to planning future large experiments such as ITER. For this purpose it is important to know the electron distribution function accurately.

In this work, we demonstrate a new numerical tool named CODE (Collisional Distribution of Electrons) that can be used for computing the electron distribution function in general and the production rate of runaway electrons in particular. These quantities are determined by a balance between acceleration in the electric field and collisions with both electrons and ions. The calculation is fully relativistic, using a collision operator valid for both low and high velocities [6] and it includes both primary and secondary runaway electron generation. If only the primary runaway electron generation is of interest, CODE can be used in both time-dependent and time-independent modes. The latter mode of operation, in which a long-time quasi-equilibrium distribution function is calculated, is extremely fast in that it is necessary only to solve a single sparse linear system. Thus, the time-independent CODE is highly suitable for coupling within larger more expensive simulations. If secondary (avalanche) generation is also considered, CODE must be run in the time-dependent mode.

Several simplifying assumptions are made in CODE. The most restrictive assumption is that spatial inhomogeneity and the associated magnetic trapping are neglected. This approximation may be justified near the magnetic axis, where most runaways are produced, since magnetic trapping becomes negligible there. The neglect of spatial inhomogeneity also means that radial transport of runaways is not included. To include these effects of spatial nonuniformity, a code such as LUKE [7, 8] or CQL3D [9, 10] must be used. Furthermore, we neglect the effect of radiation (synchrotron and bremsstrahlung) on the distribution function.

We anticipate the distribution functions computed in CODE can be used as inputs to other calculations. In this paper, we present a first example of this type, a computation of the synchrotron radiation spectrum of a runaway beam. Another possible application could be a study of instabilities driven by the anisotropy of the electron distribution function. We leave this and other possible applications for future work.

The remainder of the paper is organized as follows. In Sec. II we present the kinetic equation and the collision operator used. Section III details the discretization scheme and calculation of the primary runaway production rate, with typical results shown in section

IV. The avalanche source term and its implementation is described in Sec. V and examples of applications are given in Sec. VI. We conclude in Sec. VII.

II. KINETIC EQUATION AND NORMALIZATIONS

We begin with the kinetic equation

$$\frac{\partial f}{\partial t} + eE\mathbf{e} \cdot \nabla_{\mathbf{p}}f = C\{f\} + S. \quad (1)$$

Here, $-e$ is the electron charge, $E = |\mathbf{E}|$ is the magnitude of the electric field \mathbf{E} , $\mathbf{e} = -\mathbf{E}/E$ is a unit vector antiparallel to the electric field, $\nabla_{\mathbf{p}}$ is the gradient in the space of relativistic momentum $\mathbf{p} = \gamma m\mathbf{v}$, $\gamma = 1/\sqrt{1 - v^2/c^2}$, $v = |\mathbf{v}|$ is the speed, m is the electron rest mass, c is the speed of light, C is the electron collision operator, and S represents any sources. All quantities refer to electrons unless noted otherwise. Spatial inhomogeneity is ignored. We may write $\mathbf{e} \cdot \nabla_{\mathbf{p}}f$ in (1) in terms of scalar variables using

$$\mathbf{e} \cdot \nabla_{\mathbf{p}}f = \xi \frac{\partial f}{\partial p} + \frac{1 - \xi^2}{p} \frac{\partial f}{\partial \xi} \quad (2)$$

where $p = |\mathbf{p}|$, and $\xi = \mathbf{p} \cdot \mathbf{e}/p$ is the cosine of the pitch angle relative to the electric field. The distribution function is defined such that the density n is given by $n = \int d^3p f$, so f has dimensions of $(\text{length} \times \text{momentum})^{-3}$, and we assume the distribution function for small momentum to be approximately the Maxwellian $f_M = n\pi^{-3/2}(mv_e)^{-3} \exp(-y^2)$ where $v_e = \sqrt{2T/m}$ is the thermal speed, and $y = p/(mv_e) = \gamma v/v_e$ is the normalized momentum.

We use the collision operator from Appendix B of Ref. [6]. This operator is constructed to match the usual nonrelativistic test-particle operator in the limit of $v \ll c$, and in the relativistic limit it reduces to the operator from Appendix A of Ref. [11]. The collision operator is

$$C\{f\} = \frac{1}{p^2} \frac{\partial}{\partial p} p^2 \left[C_A \frac{\partial f}{\partial p} + C_F f \right] + \frac{C_B}{p^2} \frac{\partial}{\partial \xi} (1 - \xi^2) \frac{\partial f}{\partial \xi} \quad (3)$$

where

$$C_A = \frac{\Gamma}{v} \Psi(x), \quad (4)$$

$$C_B = \frac{\Gamma}{2v} \left[Z + \phi(x) - \Psi(x) + \frac{\delta^4 x^2}{2} \right], \quad (5)$$

$$C_F = \frac{\Gamma}{T} \Psi(x), \quad (6)$$

$\delta = v_e/c$, $x = v/v_e = y/\sqrt{1 + \delta^2 y^2}$, Z is the effective ion charge,

$$\Gamma = 4\pi n e^4 \ln \Lambda = (3\sqrt{\pi}/4)\nu_{ee}v_e^3 m^2 \quad (7)$$

is identical to the Γ defined in Refs. [6, 11, 12], $\nu_{ee} = 4\sqrt{2\pi}e^4 n \ln \Lambda / (3\sqrt{m}T^{3/2})$ is the usual Braginskii electron collision frequency, $\phi(x) = 2\pi^{-1/2} \int_0^x \exp(-s^2) ds$ is the error function, and

$$\Psi(x) = \frac{1}{2x^2} \left[\phi(x) - x \frac{d\phi}{dx} \right] \quad (8)$$

is the Chandrasekhar function. In the nonrelativistic limit $\delta \rightarrow 0$, then $y \rightarrow x$, and (3) reduces to the usual Fokker-Planck test-particle electron collision operator.

The collision operator (3) is approximate in several ways. First, it originates from the Fokker-Planck approximation in which small-angle collisions dominate, which is related to an expansion in $\ln \Lambda \gg 1$. Consequently, the infrequent collisions with large momentum exchange are ignored, so the secondary avalanche process is not included at this stage, but will be addressed later in Sec. V. Also, the modifications to the Rosenbluth potentials associated with the high-energy electrons are neglected, i.e. collisions with high-energy field particles are ignored.

The kinetic equation is normalized by multiplying through with $m^3 v_e^3 \pi^{3/2} / (\nu_{ee} n)$, and defining the normalized distribution function

$$F = (\pi^{3/2} m^3 v_e^3 / n) f \quad (9)$$

so that $F \rightarrow 1$ at $p \rightarrow 0$. We also introduce a normalized electric field

$$\hat{E} = eE / (mv_e \nu_{ee}) \quad (10)$$

which, up to a factor of order unity, is E normalized by the Dreicer field. The normalized time is $\hat{t} = \nu_{ee} t$ and the normalized source is $\hat{S} = S m^3 v_e^3 \pi^{3/2} / (\nu_{ee} n)$. We thereby obtain the dimensionless equation

$$\begin{aligned} \frac{\partial F}{\partial \hat{t}} + \hat{E} \xi \frac{\partial F}{\partial y} + \hat{E} \frac{1 - \xi^2}{y} \frac{\partial F}{\partial y} - \frac{3\sqrt{\pi}}{4} \frac{1}{y^2} \frac{\partial}{\partial y} y^2 \left[\frac{\Psi(x)}{x} \frac{\partial F}{\partial y} + 2\Psi(x)F \right] \\ - \frac{3\sqrt{\pi}}{4} \frac{1}{2xy^2} \left[Z + \phi(x) - \Psi(x) + \frac{\delta^4 x^2}{2} \right] \frac{\partial}{\partial \xi} (1 - \xi^2) \frac{\partial F}{\partial \xi} = \hat{S}. \end{aligned} \quad (11)$$

Notice that this equation has the form of a linear inhomogeneous 3D partial differential equation:

$$\frac{\partial F}{\partial \hat{t}} + MF = \hat{S} \quad (12)$$

for a linear time-independent differential operator M . If a time-independent equilibrium solution exists, it will be given by $F = M^{-1}\hat{S}$.

Since both the electric field acceleration term and the collision operator in the kinetic equation (1) have the form of a divergence of a flux in velocity space, the total number of particles is constant in time in the absence of a source: $(d/dt) \int d^3p f = \int d^3p S$. However, runaway electrons are constantly gaining energy, so without a source at small p and a sink at large p , no time-independent distribution function will exist. From another perspective, a nonzero source is necessary to find a nonzero equilibrium solution of (11), because when $\hat{S} = 0$, (11) with $\partial/\partial\hat{t} = 0$ is a homogeneous equation with homogeneous boundary conditions. (The boundary conditions are that F be regular at $y = 0$, $\xi = -1$, and $\xi = 1$, and that $f \rightarrow 0$ as $y \rightarrow \infty$.) Thus, the solution of the time-independent problem $F = M^{-1}\hat{S}$ for $\hat{S} = 0$ would be $F = 0$.

To find a solution, we must either consider a time-dependent problem or include a nonzero S . In reality, spatial transport can give rise to both sources and sinks, and a sink exists at high energy due to radiation. When included, secondary runaway generation (considered in Sec. V) also introduces a source. To avoid the added complexity of these sinks and sources and simultaneously avoid the intricacies of time dependence, when restricting ourselves to primary generation we may formulate a time-independent problem as follows. We take $\hat{S} = \alpha e^{-y^2}$ for some constant α , representing a thermal source of particles. Equation (11) for $\partial/\partial\hat{t} = 0$ may be divided through by α and solved for the unknown F/α . Then α may be determined by the requirement $F(p=0) = 1$, and F is then obtained by multiplying the solution F/α by this α .

The constant α represents the rate at which particles must be replenished at low energy to balance their flux in velocity space to high energy. Therefore, α is the rate of runaway production. As we do not introduce a sink at high energies, F will have a divergent integral over velocity space.

CODE can also be run in time-dependent mode. Once the velocity space coordinates and the operator M are discretized, any implicit or explicit scheme for advancing a system of ordinary differential equations (forward or backward Euler, Runge-Kutta, trapezoid rule, etc.) may be applied to the time coordinate. (Results shown in this paper are computed using the trapezoid rule.) Due to the diffusive nature of M , numerical stability favors implicit time-advance schemes.

III. DISCRETIZATION

We first expand F in Legendre polynomials $P_L(\xi)$:

$$F(y, \xi) = \sum_{L=0}^{\infty} F_L(y) P_L(\xi). \quad (13)$$

Then the operation

$$\frac{2L+1}{2} \int_{-1}^1 P_L(\xi) (\cdot) d\xi \quad (14)$$

is applied to the kinetic equation. Using the identities in the appendix, we obtain

$$\begin{aligned} \frac{\partial F_L}{\partial \hat{t}} + \sum_{\ell=0}^{\infty} \left\{ \hat{E} \left[\frac{L+1}{2L+3} \delta_{L+1,\ell} + \frac{L}{2L-1} \delta_{L-1,\ell} \right] \frac{\partial}{\partial y} \right. \\ \left. + \frac{\hat{E}}{y} \left[\frac{(L+1)(L+2)}{2L+3} \delta_{L+1,\ell} - \frac{(L-1)L}{2L-1} \delta_{L-1,\ell} \right] \right. \\ \left. - \frac{3\sqrt{\pi}}{4} \frac{\Psi(x)}{x} \delta_{L,\ell} \frac{\partial^2}{\partial y^2} - \frac{3\sqrt{\pi}}{2} \left[\frac{2\Psi(x)}{y} + \frac{dx}{dy} \frac{d\Psi}{dx} \right] \delta_{L,\ell} \right. \\ \left. - \frac{3\sqrt{\pi}}{4} \left[\frac{1}{x} \frac{dx}{dy} \frac{d\Psi}{dx} + \frac{2\Psi(x)}{xy} - \frac{\Psi(x)}{x^2} \frac{dx}{dy} + 2\Psi(x) \right] \delta_{L,\ell} \frac{\partial}{\partial y} \right. \\ \left. + \frac{3\sqrt{\pi}}{8xy^2} \left[Z + \phi(x) - \Psi(x) + \frac{\delta^4 x^2}{2} \right] L(L+1) \delta_{L,\ell} \right\} F_{\ell} = \hat{S}_L \end{aligned} \quad (15)$$

where $dx/dy = (1 + \delta^2 y^2)^{-3/2}$, $d\Psi/dx = 2\pi^{-1/2} e^{-x^2} - (2/x)\Psi(x)$, and $\hat{S}_L = (2L+1)2^{-1} \int_{-1}^1 \hat{S} d\xi$ is the appropriate Legendre mode of $\hat{S}(y, \xi) = \sum_{L=0}^{\infty} \hat{S}_L(y) P_L(\xi)$. Note that the collision operator is diagonal in the L index, and the electric field acceleration term is tridiagonal in L .

It is useful to examine the $L=0$ case of (15), which corresponds to (half) the integral of the kinetic equation over ξ :

$$\frac{\partial F_0}{\partial \hat{t}} - \frac{1}{y^2} \frac{\partial}{\partial y} \left[-y^2 \frac{\hat{E}}{3} F_1 + \frac{3\sqrt{\pi}}{4} y^2 \left\{ \frac{\Psi(x)}{x} \frac{\partial F_0}{\partial y} + 2\Psi(x) F_0 \right\} \right] = \hat{S}_0. \quad (16)$$

Applying $4\pi^{-1/2} \int_{y_b}^{\infty} dy y^2 (\cdot)$ for some boundary value y_b , and assuming the source is negligible in this region, we obtain

$$\frac{1}{\nu_{ee} n} \frac{dn_r}{dt} = -\frac{4}{\sqrt{\pi}} \left[-y^2 \frac{\hat{E}}{3} F_1 + \frac{3\sqrt{\pi}}{4} y^2 \left\{ \frac{\Psi(x)}{x} \frac{\partial F_0}{\partial y} + 2\Psi(x) F_0 \right\} \right]_{y=y_b} \quad (17)$$

where n_r is the number of runaways, meaning the number of electrons with $y > y_b$, so that $n_r = \int_{y>y_b} d^3p f = 2\pi \int_{mv_e y_b}^{\infty} dp p^2 \int_{-1}^1 d\xi f$. The runaway rate calculated from (17) should

be independent of y_b in steady state (as long as y_b is in a region of $\hat{S}_0 = 0$), which can be seen by applying $\int_{y_{b1}}^{y_{b2}} dy y^2(\cdot)$ to (16). We find in practice it is far better to compute the runaway production rate using (17) than from the source magnitude α , since the latter is more sensitive to the various numerical resolution parameters.

To discretize the equation in y , we can apply fourth-order finite differences on a uniform grid. Alternatively, a coordinate transformation can be applied so grid points are spaced further apart at high energies. The y coordinate is cut off at some finite maximum value y_{max} . The appropriate boundary conditions at $y = 0$ are $dF_0/dy = 0$ and $F_L = 0$ for $L > 0$. For the boundary at large y , we impose $F_L = 0$ for all L . This boundary condition creates some unphysical grid-scale oscillation at large y , which may be eliminated by adding an artificial dissipation $c_1 \exp(-[y - y_{max}]/c_2) \partial^2/\partial y^2$ localized near y_{max} to the linear operator. Suitable values for the constants are $c_1 = 0.01$ and $c_2 = 0.1$.

IV. RESULTS FOR PRIMARY RUNAWAY ELECTRON GENERATION

Figure 1 shows typical results from a time-independent CODE computation. To verify convergence, we may double $N\xi$ (the number of Legendre modes), double Ny (the number of grid points in y), and double the maximum y (y_{max}) at fixed y grid resolution (which requires doubling Ny again.) As shown by the overlap of the solid red and dashed blue curves in figure 1.a, excellent convergence is achieved for the parameters used here. As expected, the distribution function is increased in the direction opposite to the electric field ($p_{\parallel} > 0$). While the distribution function is reduced in the direction parallel to the electric field ($p_{\parallel} < 0$) for $y < 5$, F is actually slightly increased for $y > 5$ due to pitch-angle scattering of the high-energy tail electrons [13]. This interpretation can be confirmed by suppressing the pitch-angle scattering term in CODE, in which case F is reduced in the direction parallel to the electric field for all y .

Figure 2 compares the distribution functions obtained from the time-independent and time-dependent approaches. At sufficiently long times, the time-dependent version produces results that are indistinguishable from the time-independent version.

For comparison with previously published results, we show in Figure 3 results by Kulsrud et al [14], who considered only the nonrelativistic case $\delta \rightarrow 0$. The agreement with CODE is exceptional. The runaway production rate in CODE is computed using (17) for $y_b = 10$.

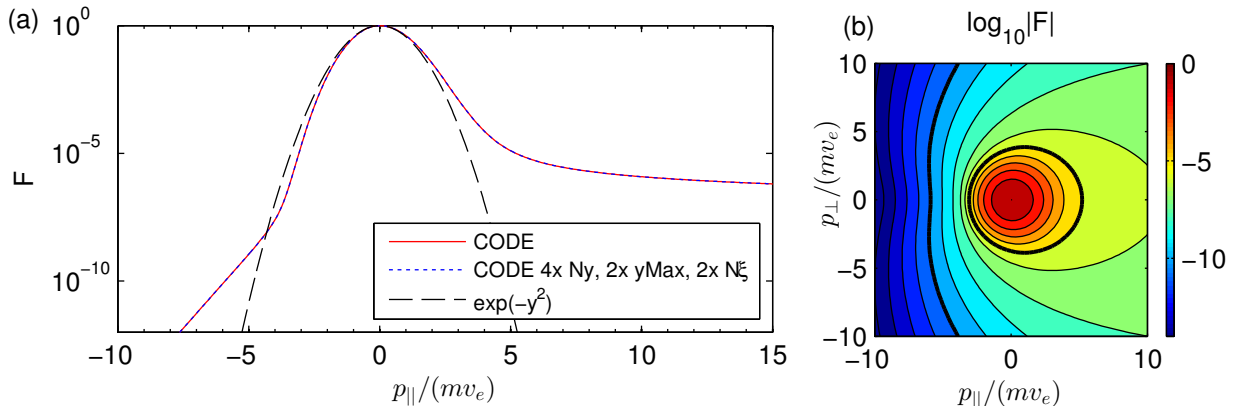


FIG. 1: (Color online) Typical results of CODE, obtained for $\delta = 0.1$, $\hat{E} = 0.1$, and $Z = 1$. (a) Normalized distribution function F for $p_{\perp} = 0$. Results are plotted for two different sets of numerical parameters ($\{Ny = 300, y_{max} = 20, N\xi = 20\}$ and $\{Ny = 1200, y_{max} = 40, N\xi = 40\}$). The results overlap completely, demonstrating excellent convergence. A Maxwellian is also plotted for comparison. (b) Contours of F at values 10^z for integer z . Bold contours indicate $F = 10^{-5}$ and 10^{-10} .

(Any value of $y_b > 5$ gives indistinguishable results.) Ref. [14] uses a different normalized electric field E_K which is related to \hat{E} by $E_K = 2(3\sqrt{\pi})^{-1}\hat{E}$, and in Ref. [14] the runaway rate is also normalized by a different collision frequency $\nu_K = 3\sqrt{\pi/2}\nu_{ee}$. It should also be noted that the Kulsrud computations are time-dependent, with a simulation run until the flux in velocity space reaches an approximate steady state. Each CODE point shown in figure 3 took approximately 0.08s on a single Dell Precision laptop with Intel Core i7-2860 2.50 GHz CPU and 16 GB memory, running in MATLAB. Faster results could surely be obtained using a lower-level language.

V. SECONDARY RUNAWAY ELECTRON GENERATION

In the previous sections we used the Fokker-Planck collision operator, which includes “distant” (large impact parameter) collisions but not “close” (small impact parameter) collisions in which a large fraction of energy and momentum are transferred between the colliding particles. Close collisions are infrequent compared to distant collisions, and are therefore neglected in the Fokker-Planck operator. However, close collisions may still have a significant effect on runaway generation, since the density of runaways is typically much smaller than

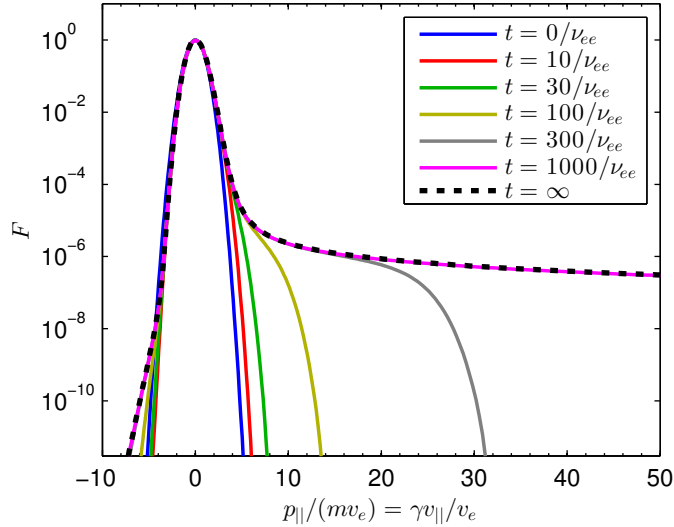


FIG. 2: (Color online) The distribution function from time-dependent CODE at various times. At $t = 1000/\nu_{ee}$, the distribution function is indistinguishable from the solution obtained using the time-independent scheme ($t = \infty$) over the momentum range shown.

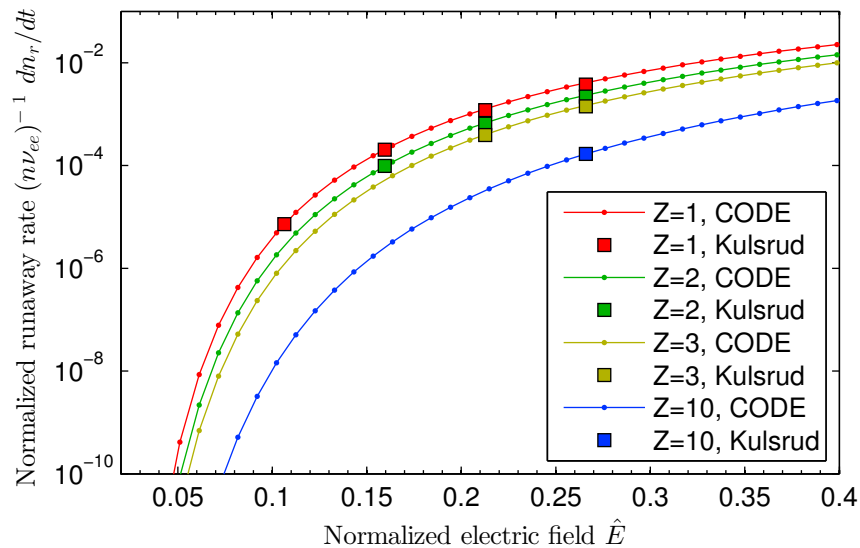


FIG. 3: (Color online) Benchmark of CODE in the nonrelativistic limit $\delta \rightarrow 0$ against data in Table 1 of Ref. [14].

the density of thermal electrons which may be accelerated in a close collision. The production of runaways through close collisions is known as secondary production, or as avalanche production since it may occur with exponential growth. To simulate secondary generation of energetic electrons, we use a source term derived in [15], starting from the Møller scattering

cross-section in the $w \gg 1$ limit, with $w = p/(mc) = \delta y$ a normalized momentum. In this limit, the trajectories of the primary electrons are not much deflected by the collisions. The source then takes the form

$$S = \frac{n_r}{4\pi\tau \ln \Lambda} \delta(\xi - \xi_2) \frac{1}{w^2} \frac{\partial}{\partial w} \left(\frac{1}{1 - \sqrt{1 + w^2}} \right), \quad (18)$$

where $1/\tau = 4\pi n e^4 \ln \Lambda / (m^2 c^3)$ is the collision frequency for relativistic electrons, n_r is the density of the fast electrons and $\xi_2 = w / (1 + \sqrt{1 + w^2})$ is the cosine of the pitch angle at which the runaway is born. (Our (18) differs by a factor $m^3 c^3$ compared to the source in Ref. [15] since we normalize our distribution function as $n = \int d^3 p f$ instead of $n = \int d^3 w f$. There is also a factor of 2π difference due to the different normalization of the distribution function.)

Due to the approximations used to derive S , care must be taken in several regards. First, to define n_r in (18), it is not clear where to draw the dividing line in velocity space between runaways and non-runaways. One possible strategy for defining n_r is to compute the separatrix in velocity space between trajectories that will have bounded and unbounded energy in the absence of diffusion, and to define the runaway density as the integral of f over the latter region [16]. This approach may somewhat overestimate the true avalanche rate, since it neglects the fact that some time must elapse between an electron entering the runaway region and the electron gaining sufficient energy to cause secondary generation. As most runaways have $\xi \approx 1$, we may approximate the separatrix by setting $dw/dt = 0$ where $dw/dt = eE/(mc) - (1 + 1/w^2)/\tau$ defines the trajectory of a particle with $\xi = 1$, neglecting diffusion in momentum and pitch angle. The runaway region is therefore $w > w_c$ where $w_c = [(E/E_c) - 1]^{-1/2}$ and $E_c = e\tau/(mc)$ is the critical field, and so we take $n_r = 2\pi m^3 c^3 \int_{-1}^1 d\xi \int_{w_c}^{\infty} dw w^2 f$. (We cannot define n_r by the time integral of (17), since (17) is no longer valid when S is nonzero away from $p \approx 0$.) A second deficiency of (18) is that S is singular at $w \rightarrow 0$, so the source must be cut off below some threshold momentum. Following Ref. [10], we choose the cutoff to be w_c . Neither of the cutoffs discussed here would be necessary if a less approximate source term than (18) were used, but derivation of such an operator is beyond the scope of this paper.

Normalizing and applying (14) as we did previously for the other terms in the kinetic equation, the source included in CODE becomes

$$\hat{S}_L = \frac{n_r}{n} \frac{3\pi\delta^5}{16 \ln \Lambda} \frac{2L + 1}{2} P_L(\xi_2) \frac{1}{(1 - \sqrt{1 + w^2})^2 \sqrt{1 + w^2} y}. \quad (19)$$

When secondary generation is included, CODE must be run in time-dependent mode.

To benchmark the numerical solution of the kinetic equation including the above source term by CODE, we use the approximate analytical expression for the avalanche distribution function derived in Section II of Ref. [17]:

$$f_{aa}(w_{\parallel}, w_{\perp}) = \frac{k}{w_{\parallel}} \exp \left(\tilde{\gamma}t - \frac{\tilde{\gamma}\tau}{E/E_c - 1} w_{\parallel} - \left[\frac{E/E_c - 1}{Z + 1} \right] \frac{w_{\perp}^2}{2w_{\parallel}} \right) \quad (20)$$

where k is a constant. The quantity $\tilde{\gamma}$ is the growth rate $\tilde{\gamma} = (1/f)\partial f/\partial t$, which must be independent of both time and velocity for (20) to be valid. Equation (20) is also valid only where $p_{\parallel} \gg p_{\perp}$ and in regions of momentum space where S is negligible. (This restriction is not a major one since $S = 0$ everywhere except on the $\xi = \xi_2$ curve.) If most of the runaway distribution function is accurately described by (20), then we may approximate $n_r \approx \int d^3p f_{aa} = 2\pi m^3 c^3 \int_{-\infty}^{\infty} dw_{\parallel} \int_0^{\infty} dw_{\perp} w_{\perp} f_{aa}$, giving $\tilde{\gamma} = (1/n_r)dn_r/dt$ and

$$k = n_r e^{-\tilde{\gamma}t} \frac{\tau}{2\pi m^3 c^3 (1 + Z)} \quad (21)$$

where $n_r e^{-\tilde{\gamma}t}$ is constant. (Equation (21) may be inaccurate in some situations even if (20) is accurate in part of velocity-space, because (21) requires (20) to apply in *all* of velocity-space.) Figures 4 and 5 show comparisons between distributions from CODE and (20)-(21) for two different sets of parameters. More precisely, the quantity plotted in figures 4-5 is $\log_{10}(m^3 c^3 f/n_r)$. To generate the figures, CODE is run for a sufficiently long time that $(1/f)\partial f/\partial t$ becomes approximately constant. The resulting numerical value of $(1/n_r)dn_r/dt$ is then used as $\tilde{\gamma}$ when evaluating (20)-(21). For a cleaner comparison between CODE and analytic theory in these figures, we minimize primary generation in CODE in these runs by initializing f to 0 instead of to a Maxwellian. For both sets of physical parameters, the agreement between CODE and (20) is excellent in the region where agreement is expected: where $p_{\parallel} \gg p_{\perp}$ and away from the curve $\xi = \xi_2$.

VI. APPLICATIONS

As an application of the distribution functions calculated by CODE, we consider the synchrotron radiation emitted by runaway electrons in a magnetized plasma as a result of their gyromotion. Synchrotron emission is a useful diagnostic for runaways, since due to the energy dependence of the emitted synchrotron power, the emission from runaways

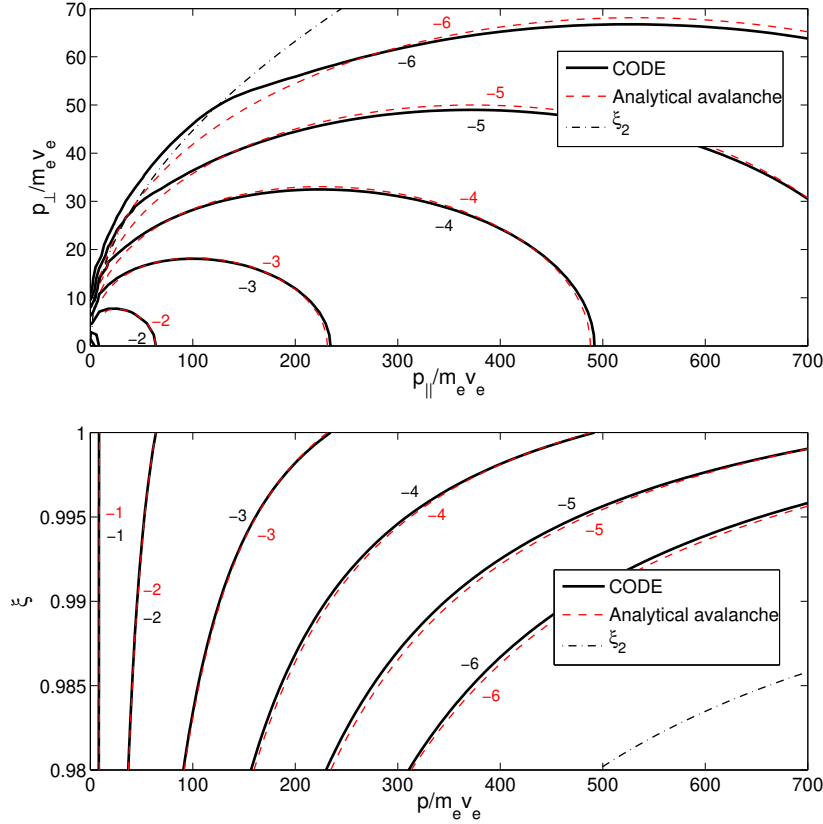


FIG. 4: (Color online) Contour plots of the long-time distribution function from CODE (shown in two different coordinate systems), obtained for $E/E_c = 40$ ($\hat{E} = 0.532$), $Z = 3$, $\delta = 0.1$ and $t = 5000/\nu_{ee}$. Results are plotted for the numerical parameters $Ny = 1500$, $y_{max} = 1500$ and $N\xi = 100$, with time step $dt = 10/\nu_{ee}$. The analytical distribution in (20)-(21) for the same physical parameters is also plotted for comparison, together with part of the curve where avalanche runaways are created ($\xi = \xi_2$).

completely dominates that of the thermal particles. The emission also depends strongly on the pitch-angle of the particle. In a cylindrical plasma geometry, the emitted synchrotron power per wavelength at wavelength λ from a single highly energetic particle is given by [18]

$$\mathcal{P}(\gamma, \gamma_{\parallel}, \lambda) = \frac{4\pi}{\sqrt{3}} \frac{ce^2}{\lambda^3 \gamma^2} \int_{\lambda_c/\lambda}^{\infty} K_{5/3}(l) dl, \quad (22)$$

where the two-dimensional momentum of the particle is determined by γ and $\gamma_{\parallel} = 1/\sqrt{1 - v_{\parallel}^2/c^2}$, $K_{\nu}(x)$ is a modified Bessel function of the second kind, and

$$\lambda_c = \frac{4\pi}{3} \frac{mc^2 \gamma_{\parallel}}{eB\gamma^2}, \quad (23)$$

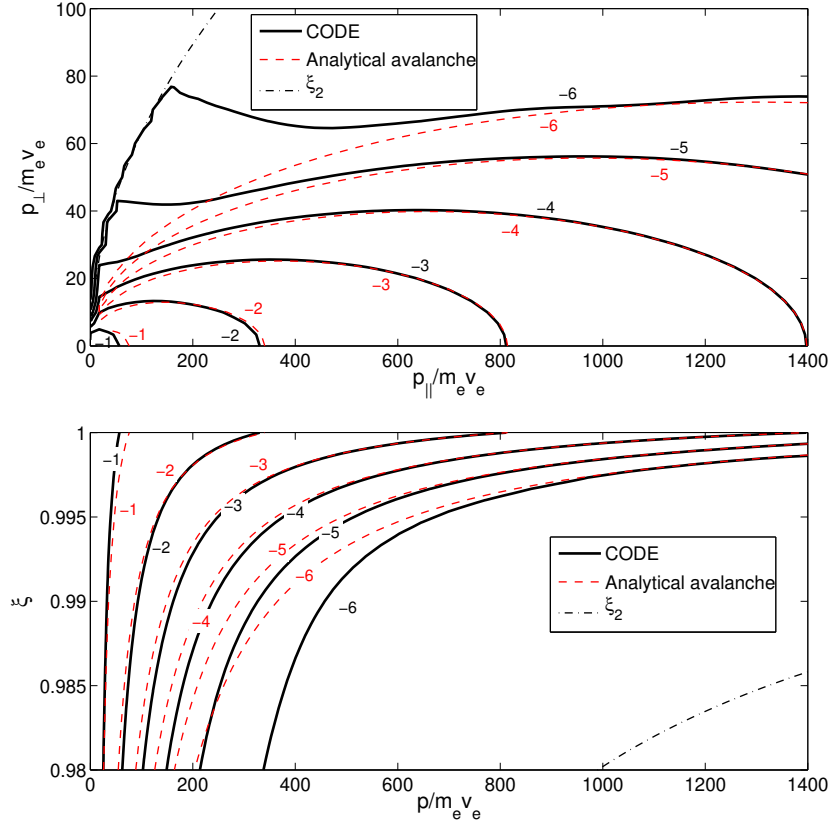


FIG. 5: (Color online) Contour plots of the long-time distribution function from CODE (shown in two different coordinate systems), obtained for $E/E_c = 100$ ($\hat{E} = 0.332$), $Z = 1$, $\delta = 0.05$ and $t = 6000/\nu_{ee}$. Results are plotted for the numerical parameters $Ny = 1500$, $y_{max} = 3000$ and $N\xi = 180$, with time step $dt = 25/\nu_{ee}$. The analytical distribution in (20)-(21) is also plotted for comparison, together with part of the curve where avalanche runaways are created ($\xi = \xi_2$).

where B is the magnetic field strength.

Using CODE we will demonstrate that the synchrotron radiation spectrum from the entire runaway distribution is substantially different from the spectrum obtained from a single particle approximation. By transforming to the more suitable coordinates w and ξ , related to γ and γ_{\parallel} through $\gamma^2 = 1 + w^2$ and $\gamma_{\parallel}^2 = (1 - w^2\xi^2/(1 + w^2))^{-1}$, and integrating (22) over the runaway region R in momentum space, we obtain the total synchrotron emission from the runaway distribution. Normalizing to n_r , we find that the average emitted power per runaway particle at a wavelength λ is given by

$$P(\lambda) = \frac{2\pi}{n_r} \int_R f(w, \xi) \mathcal{P}(w, \xi, \lambda) w^2 dw d\xi . \quad (24)$$

The per-particle synchrotron spectra generated by the CODE distributions in Figures 4 and 5 were calculated using this formula, and are shown in Figure 6, together with the spectra radiated by electron distributions for other electric field strengths. For the physical parameters used, we note that the peak emission occurs between 10 and 20 μm . The synchrotron spectra show a decrease in per-particle emission with increasing electric field strength. Even though a stronger electric field leads to more particles with high energy (and thus high average emission), it also leads to a more narrow distribution in pitch-angle. This reduction in the number of particles with large pitch-angle leads to a decrease in average emission. Both figures confirm that the average emission is reduced for higher electric fields, implying that the latter mechanism has the largest impact on the spectrum.

In calculating the spectra, the runaway region of momentum space, R , was defined such that the maximum particle momentum was $w_{\text{max}} = 50$ (which translates to $y_{\text{max}} = 500$ and $y_{\text{max}} = 1000$ respectively for the cases shown in Figures 4 and 5), corresponding to a maximum particle energy of $\simeq 25$ MeV. Physically the cutoff at large energy can be motivated by the finite life-time of the accelerating electric field and the influence of loss mechanisms such as radiation. Since the radiated synchrotron power increases with both particle energy and pitch, this truncation of the distribution is necessary to avoid infinite emission, although the precise value for the cutoff depends on the tokamak and on discharge-specific limitations to the maximum runaway energy. For the lower bound of R , $w_{\text{min}} = w_c = [(E/E_c) - 1]^{-1/2}$ was used, and all particles with $\xi \in [0, 1]$ were included. Although no explicit cutoff was imposed in ξ , the distribution decreases rapidly as this parameter decreases from 1 (as can be seen in Figures 4 and 5) and there are essentially no particles below some effective cutoff value.

Figure 6 also shows the synchrotron spectrum from a single particle with momentum corresponding to the maximum momentum of the distributions ($w = 50$), and pitch-angle $y_{\perp}/y_{\parallel} = 0.2$, which is qualitatively consistent with measurements of the maximum runaway pitch on Textor [19] and DIII-D [20]. This choice is equivalent to using a 2D δ -function approximation of the distribution, as was done in Refs. [19, 21] (and with some modification in [20]). The figure shows that using this approximation overestimates the synchrotron emission per particle by several orders of magnitude. Note that in the figure, the values for the emitted power per particle were divided by a large number to fit in the same scale. The overestimation is not surprising, since the δ -function approximation assumes that all

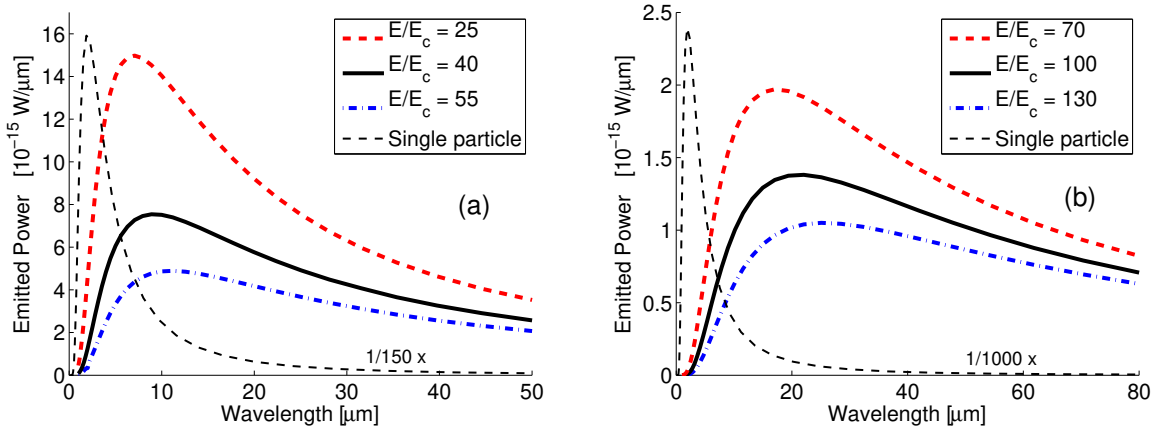


FIG. 6: (Color online) Synchrotron spectra (average emission per particle) for the runaway distributions in (a) Figure 4 and (b) Figure 5. Emission spectra from the CODE distributions in Figures 4 and 5 are shown in solid black, together with spectra from distributions with varying electric field strength but otherwise identical physical parameters. A magnetic field of $B = 3$ T was used. The synchrotron spectrum from a single particle with $w = 50$ and $y_{\perp}/y_{\parallel} = 0.2$ is also shown. (This spectrum is the same in both cases, as the particle parameters are independent of simulation settings).

particles emit as much synchrotron radiation as the most strongly emitting particle in the actual distribution. The figure also shows that the wavelength of peak emission is shifted towards shorter wavelengths when using the δ -function approximation. In order to obtain an accurate runaway synchrotron spectrum, it is thus crucial to use the full runaway distribution in the calculation.

In principle, we may also use the synchrotron spectra from distributions calculated through CODE to estimate the maximum energy of the runaways in existing tokamaks. However, due to the region of sensitivity of the available detectors, there is only a limited wavelength range in which calculated spectra can be fitted to experimental data in order to determine the maximum runaway energy. The available range often corresponds to the short wavelength slope of the spectrum, where the emitted power shows an approximately linear dependence on wavelength. Indeed, the short-wavelength spectrum slope has been used to estimate the maximum runaway energy in experiments [19]. If the runaway distribution function is approximated by a δ -function at the maximum available energy and pitch angle, there is a monotonic relationship between the short-wavelength spectrum slope

and the maximum particle energy (at fixed pitch angle). Such a relationship holds because increasing the particle energy leads to more emission at shorter wavelengths, resulting in a shift of the wavelength of peak emission towards shorter wavelengths, and a corresponding change in the spectrum slope.

Using an integrated synchrotron spectrum from a CODE distribution is much more accurate than the single particle approximation, but also introduces additional parameters (\hat{E} , δ , Z). If the physical parameters are well known, a unique relation still holds between the spectrum slope and the maximum particle energy. During disruptions however, many parameters (like the temperature and the effective charge) are hard to measure with accuracy. As the shape of the underlying distribution depends on the values of the parameters, the synchrotron spectrum will do so as well. This complexity is apparent in Figure 6, where the single particle approximation produces identical results in the two cases, whereas the spectra from the complete distributions are widely different. The dependence on distribution shape makes it possible in principle for two sets of parameters to produce the same spectrum slope for different maximum energies. Given this insight, using the complete runaway distribution when modelling experimentally obtained spectra is necessary for an accurate analysis and reliable fit of the maximum particle energy. In this context, CODE is a very useful tool with the possibility to contribute to the understanding of runaways and their properties.

In providing the electron distribution functions (and thus knowledge of a variety of quantities through its moments), the applicability of CODE is wide, and the potential in coupling CODE to other software, e.g. for modelling of runaway dynamics in disruptions, is promising. For a proper description of the runaways generated in disruptions it is important to take into account the evolution of the radial profiles of the electric field and fast electron current self-consistently. This can be done by codes such as GO, initially described in Ref. [22] and developed further in Refs. [23, 24]. GO solves the equation describing the resistive diffusion of the electric field in a cylindrical approximation coupled to the runaway generation rates. In the present version of GO, the runaway rate is computed by approximate analytical formulas for the primary and secondary generation. Using CODE, the analytical formulas can be replaced by a numerical solution for the runaway rate which would have several advantages. One advantage would be that Dreicer, hot-tail and secondary runaways could all be calculated with the same tool, avoiding the possibilities for double-counting and difficulties with interpretations of the results. Also, in the present version of GO, it is

assumed that all the runaway electrons travel at the speed of light, an approximation that can be easily relaxed using CODE, which calculates the electron distribution in both energy and pitch-angle. Most importantly, the validity region of the results would be expanded, as the analytical formulas are derived using various assumptions which are often violated in realistic situations. The output would be a self-consistent time and space evolution of electric field and runaway current, together with the electron distribution function. This information can then be used for calculating quantities that depend on the distribution function, such as the synchrotron emission or the kinetic instabilities driven by the velocity anisotropy of the runaways.

VII. CONCLUSIONS

The CODE code provides a fast computation of the runaway electron distribution function. Both primary (Dreicer) and secondary (avalanche) generation are included. A Legendre spectral discretization is applied to the pitch-angle coordinate, with high-order finite differences applied to the speed coordinate. A nonuniform speed grid allows high resolution of thermal particles at the same time as a high maximum energy without a prohibitively large number of grid points. If secondary generation is negligible, the long-time distribution function may be calculated by solving a single sparse linear system. The speed of the code makes it feasible to couple to other codes for integrated modelling of complex processes such as tokamak disruptions. CODE has been benchmarked against previous analytic and numerical results in appropriate limits, showing excellent agreement.

As an example application, we investigated the synchrotron radiation spectra from runaway electron distributions. We found that the radiation spectrum from a single electron can differ substantially from the overall spectrum generated by a distribution of electrons. Therefore, experimental estimates of maximum runaway energy based on the single-particle synchrotron spectrum are likely to be inaccurate. A detailed study of the distribution-integrated synchrotron spectrum and its dependencies on physical parameters will be presented in a future publication.

We also note in closing that the applicability of CODE is not limited to modelling fusion plasmas. CODE could be useful also in modelling of the fast electron dynamics in laser-plasma accelerators, where the electric field evolution could be given by a Particle-In-

Cell (PIC) code. CODE may also be useful for modelling fast electrons in lightning or in astrophysical applications.

Acknowledgments

This work was supported by the Fusion Energy Postdoctoral Research Program administered by the Oak Ridge Institute for Science and Education, and by the European Communities under Association Contract between EURATOM and *Vetenskapsrådet*. The views and opinions expressed herein do not necessarily reflect those of the European Commission. The authors are grateful to G. Papp, J. Decker, and Y. Peysson for fruitful discussions.

Appendix A: Integrals of Legendre Polynomials

Here we describe several identities for Legendre polynomials which are required for the spectral pitch-angle discretization. To evaluate the ξ integral of the $\xi \partial F / \partial y$ term in (11), we use the recursion relation

$$\xi P_L(\xi) = \frac{L+1}{2L+1} P_{L+1}(\xi) + \frac{L}{2L+1} P_{L-1}(\xi) \quad (\text{A1})$$

where P_{L-1} is replaced by 0 when $L = 0$. Applied to the relevant integral in (11), and noting the orthogonality relation $(2L+1)2^{-1} \int_{-1}^1 P_L(\xi) P_\ell(\xi) d\xi = \delta_{L,\ell}$, we find

$$\frac{2L+1}{2} \int_{-1}^1 d\xi \xi P_L(\xi) P_\ell(\xi) = \frac{L+1}{2L+3} \delta_{\ell,L+1} + \frac{L}{2L-1} \delta_{\ell,L-1}. \quad (\text{A2})$$

Similarly, to evaluate the ξ integral of the $\partial F / \partial \xi$ term in (11), we use the recursion relation

$$(1 - \xi^2)(dP_L/d\xi) = LP_{L-1}(\xi) - L\xi P_L(\xi) \quad (\text{A3})$$

to obtain

$$\frac{2L+1}{2} \int_{-1}^1 d\xi P_L(\xi)(1 - \xi^2) \frac{dP_\ell}{d\xi} = \frac{(L+1)(L+2)}{2L+3} \delta_{\ell,L+1} - \frac{(L-1)L}{2L-1} \delta_{\ell,L-1}. \quad (\text{A4})$$

Finally, the pitch-angle scattering collision term gives the integral

$$\frac{2L+1}{2} \int_{-1}^1 d\xi P_L(\xi) \frac{\partial}{\partial \xi} (1 - \xi^2) \frac{\partial}{\partial \xi} P_\ell(\xi) = -(L+1)L \delta_{L,\ell}. \quad (\text{A5})$$

[1] H. Dreicer, Phys. Rev. **117**, 329 (1960).

- [2] J. W. Connor and R. J. Hastie, Nucl. Fusion **15**, 415 (1975).
- [3] H. P. Furth and P. H. Rutherford, Phys. Rev. Lett. **28**, 545 (1972).
- [4] P. Helander and D. Ward, Phys. Rev. Lett. **90**, 135004 (2003).
- [5] T. Fülöp and G. Papp, Phys. Rev. Lett. **51**, 043004 (2012).
- [6] G. Papp, M. Drevlak, T. Fülöp, and P. Helander, Nucl. Fusion **51**, 043004 (2011).
- [7] Y. Peysson, J. Decker, and R. W. Harvey, AIP Conf. Proc. **694**, 495 (2003).
- [8] Y. Peysson and J. Decker, AIP Conf. Proc. **1069**, 176 (2008).
- [9] S. C. Chiu, M. N. Rosenbluth, R. W. Harvey, and V. S. Chan, Nucl. Fusion **38**, 1711 (1998).
- [10] R. W. Harvey, V. S. Chan, S. C. Chiu, T. E. Evans, and M. N. Rosenbluth, Phys. Plasmas **7**, 4590 (2000).
- [11] P. Sandquist, S. E. Sharapov, P. Helander, and M. Lisak, Phys. Plasmas **13**, 072108 (2006).
- [12] C. Karney and N. Fisch, Phys. Fluids **28**, 116 (1985).
- [13] Y. Peysson and J. Decker, Personal communication (2013).
- [14] R. M. Kulsrud, Y.-C. Sun, N. K. Winsor, and H. A. Fallon, Phys. Rev. Lett. **31**, 690 (1973).
- [15] M. N. Rosenbluth and S. V. Putvinski, Nucl. Fusion **37**, 1355 (1997).
- [16] H. Smith, P. Helander, L.-G. Eriksson, and T. Fülöp, Phys. Plasmas **12**, 122505 (2005).
- [17] T. Fülöp, G. Pokol, P. Helander, and M. Lisak, Phys. Plasmas **13**, 062506 (2006).
- [18] G. Bekefi, *Radiation Processes in Plasmas* (Wiley, 1966).
- [19] R. Jaspers, N. J. L. Cardozo, A. J. H. Donné, H. L. M. Widdershoven, and K. H. Finken, Rev. Sci. Instrum. **72**, 466 (2001).
- [20] J. H. Yu, E. M. Hollmann, N. Commaux, N. W. Eidietis, D. A. Humphreys, A. N. James, T. C. Jernigan, and R. A. Moyer, Phys. Plasmas **20**, 042113 (2013).
- [21] K. H. Finken, J. G. Watkins, D. Rusbuldt, W. J. Corbett, K. H. Dippel, D. M. Goebel, and R. A. Moyer, Nucl. Fusion **30**, 859 (1990).
- [22] H. Smith, P. Helander, L.-G. Eriksson, D. Anderson, M. Lisak, and F. Andersson, Phys. Plasmas **13**, 102502 (2006).
- [23] K. Gál, T. Fehér, H. Smith, T. Fülöp, and P. Helander, Plasma Phys. Controlled Fusion **50**, 055006 (2008).
- [24] T. Fehér, H. M. Smith, T. Fülöp, and K. Gál, Plasma Phys. Controlled Fusion **53**, 035014 (2011).